Aerospace Science and Technology 14 (2010) 459–471

Contents lists available at ScienceDirect

Aerospace Science and Technology

www.elsevier.com/locate/aescte

On-ground aircraft control design using a parameter-varying anti-windup approach

Clément Roos [a,*], Jean-Marc Biannic [a], Sophie Tarbouriech [b], Christophe Prieur [b], Matthieu Jeanneau [c]

[a] ONERA, System Control and Flight Dynamics Department, 2 avenue Edouard Belin, F-31055 Toulouse Cedex 4, France
[b] LAAS-CNRS, Methods and Algorithms in Control Group, University of Toulouse, 7 avenue du Colonel Roche, F-31077 Toulouse Cedex 4, France
[c] AIRBUS, 316 route de Bayonne, F-31060 Toulouse Cedex 9, France

ARTICLE INFO

Article history:
Received 20 January 2009
Received in revised form 23 December 2009
Accepted 18 February 2010
Available online 21 February 2010

Keywords:
Saturations
Dynamic anti-windup design
Parameter-varying systems
Linear fractional transformation (LFT) modeling
On-ground aircraft

ABSTRACT

As an original alternative to dynamic inversion techniques, a non-standard anti-windup control strategy is developed in this paper in order to improve the on-ground control system of a civilian aircraft. Using a linear fractional representation (LFR) of the aircraft in combination with an original approximation of the nonlinear ground forces by saturation-type nonlinearities, the proposed design method delivers low-order and robust controllers, which are automatically adapted to the runway state and to the aircraft longitudinal velocity. The efficiency of the design scheme is assessed by several nonlinear simulations.

1. Introduction

Fly-by-wire systems are now commonly used on-board transport aircraft. They allow the automation of many parts of the flight, including the highly nonlinear landing phase. This automation significantly reduces the piloting workload that traditionally required the full attention of pilots, such as navigation tasks, weather watch, air traffic communications and on-board activities monitoring. This is permitted by the fly-by-wire laws that control the airplane and ensure that it follows some precise orders. In addition, some flight-domain protections contribute to enhancing the safety of flights by preventing from entering abnormal conditions. Aircraft manufacturers work in close collaboration with academics in order to integrate some modern control techniques to their process, making today fly-by-wire control laws highly reliable, robust and efficient. In the past years, enhanced functionalities such as turbulence or gust alleviation have thus been introduced, allowing increased comfort in flight, but also decreased structural loads on the airframes.

On the other hand, aircraft on-ground control remains very limited and mainly consists of heading and velocity control once aligned on the runway before take-off or after touch-down. It is performed without explicit control of the pilot and the dedicated control laws are quite simple compared to those developed for the flight phases: they do not offer the same protections of the normal operating envelope, and robustness to external disturbances or variation in the runway state is not ensured. Moreover, apart for keeping the aircraft on the runway, all turns and maneuvers on ground are directly performed by the pilots using manual open-loop control. This difference between in-flight and on-ground control can be explained easily. Aerodynamics and their impact on handling qualities have been extensively studied in the past. But the on-ground motion is more complex due to the coupling between aerodynamics and friction forces between the wheels and the ground, the latter being highly nonlinear and depending on many external parameters. Of course, right after touchdown, the aerodynamic effects are dominating, while on the taxiway the main concern is ground forces. Nevertheless, the coupling between the two is high during the acceleration and deceleration phases. Moreover, the effects of wind or gusts are amplified by the aerodynamic characteristics of the aircraft, and they significantly impact the ground forces and the motion along the runway or the taxiway.

Air transport has experienced several runway overruns in the past years. A first benefit of using an autopilot to automate the on-ground motion would thus be to improve the safety during airport operations whatever the visibility, rain, wind or gust. But there is also an economic benefit. Indeed, the longitudinal distances between aircraft currently need to be increased in bad weather conditions. And managing the on-ground traffic requires additional safety margins in case of fog. In this context, the automation of the on-ground motion appears as a prerequisite to

* Corresponding author. Tel.: +33 5 62 25 29 25; fax: +33 5 62 25 25 64.
E-mail address: clement.roos@onera.fr (C. Roos).

1270-9638/$ – see front matter
doi:10.1016/j.ast.2010.02.004

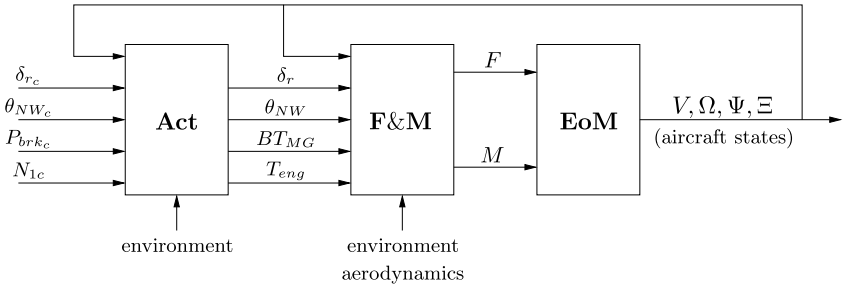

Fig. 1. General architecture of the initial nonlinear model.

a more autonomous on-ground traffic and to increased airports traffic capabilities. These requirements are pushing for developing enhanced on-ground control functionalities. The first step consists in developing robust ground-by-wire control laws, so as to pilot the lateral load factor N_y or the yaw rate r for the lateral motion, and the longitudinal load factor N_x or the ground velocity V_x for the longitudinal motion. The second step is then to develop autonomous navigation, such as runway exit at the right speed while minimizing the occupation time, or autonomous motion along the taxiways towards the selected gate for instance. These last tasks can be performed by computing the right orders to send to the ground-by-wire control laws. The most challenging aspect today, which is investigated in this paper, is thus the first step: being able to provide a safe, robust and reliable on-ground control of an airplane in the highly nonlinear and fast varying context of the on-ground motion.

A preliminary solution based on a nonlinear (NL) dynamic inversion technique was proposed in [10] to control the lateral motion of an on-ground aircraft. More precisely, it was shown in this paper that linear methods could not be directly applied for this specific control application. An alternative solution is proposed here, which consists in reducing the highly nonlinear interactions between the tyres and the ground to saturation-type nonlinearities. The resulting control issue thus falls within the scope of anti-windup techniques. In this context, a dynamic anti-windup design method based on modified sector conditions [13] is proposed to optimize a newly introduced performance level for saturated systems [8]. The extension to parameter-varying systems is also highlighted. Interestingly, the problem is shown to be convex for the considered application. As a result, the anti-windup gains are easily computed. Moreover, it is shown that the saturation levels, which depend on the runway state, can be identified on-line, and that the resulting estimator can be written as an LFR. This enables a clever adaptation of the performance levels. The present contribution should thus be read as a non-standard application of anti-windup control, which is here an original alternative to dynamic inversion.

The paper is organized as follows. A high-fidelity nonlinear on-ground aircraft model developed in an industrial context is succinctly described in Section 2 and a simplified design-oriented LFR is derived in Section 3. The proposed control strategy is stated in Section 4, while Section 5 is devoted to the presentation of some new results regarding anti-windup design and to the way they can be extended to handle parameter-varying plants. Section 6 then details both the design process on the simplified model and the controller implementation on the full nonlinear plant. Several simulations are performed, which demonstrate the significant improvements induced by the anti-windup compensator. Concluding remarks are presented in Section 7, which also provides directions for future works.

2. Description of the high-fidelity on-ground aircraft model

2.1. General architecture

The open-loop nonlinear model presented in this section describes the on-ground dynamics of an Airbus transport aircraft with two engines. It is representative of the aircraft behavior from touchdown to complete stop and can be represented by three main blocks of differential equations, as shown in Fig. 1.

The **EoM** block contains the equations of motion and is generic for all aircraft (on-ground and airborne). Its inputs are the total forces F and moments M and its outputs are the twelve standard aircraft degrees of freedom, namely the linear and angular positions (Ψ and Ξ) and velocities (V and Ω). As an example, the evolution of $V = [V_x\ V_y\ V_z]^T$ and $\Omega = [p\ q\ r]^T$ is described by:

$$\begin{bmatrix} \dot{V} \\ \dot{\Omega} \end{bmatrix} = \begin{bmatrix} \frac{F}{m} - \Omega \wedge V \\ I^{-1}(M - \Omega \wedge (I.\Omega)) \end{bmatrix} \tag{1}$$

where I is the inertia matrix and m the aircraft mass.

The main forces $F = [F_x\ F_y\ F_z]^T$ and moments $M = [M_x\ M_y\ M_z]^T$ acting on the aircraft are modeled in the **F&M** block and correspond to the aerodynamic effects, the gravity, the engines thrust and the ground forces. They depend on several aerodynamic and environmental data, but also on the positions of the actuators (rudder deflection δ_r, nose wheel angular position θ_{NW}, braking torque at main landing gear BT_{MG} and engine thrust T_{eng}). The aerodynamic coefficients C_x, C_y and C_z are modeled by neural networks. But the most specific and important contribution comes from the ground forces F_{ground}, which are induced by the interactions (wheel slip, rolling drag, braking forces) between the nose wheel (NW) and main landing gear (MG) tyres and the ground. Their computation is quite complex because they are highly nonlinear functions of the local sideslip angles β_{NW} and β_{MG}, but also of the vertical load F_z, the runway state (dry, wet or icy) and the aircraft longitudinal velocity V_x. A macroscopic nonlinear model is used which combines various elements from [2,3].

The **Act** block contains the actuators models. It is composed of three nonlinear subsystems associated to the nose wheel steering system, the braking system and the engines.

2.2. Need for a simplified model

The nonlinear model presented in Section 2.1 is described by differential equations. It is not directly compatible with the anti-windup design tools developed in Section 5, which require the considered plant to be written as an LFR.[1] A first method is to convert it using the nonlinear symbolic LFT modeling approach

[1] Basically, building an LFR consists in transforming the initial system into a time-invariant plant $M(s)$ in feedback loop with a block diagonal operator Δ, which contains all the nonlinearities, the varying parameters and the uncertainties of the system. A good introduction to LFT modeling can be found in [17].

proposed in [19]. An exact representation is then obtained, whose Δ block is a 201×201 matrix [20]. Nevertheless, such a representation is intractable for control laws development because of its high complexity. A better alternative consists in simplifying the initial nonlinear model before trying to put it under an LFT form. Both the simplifying assumptions and the strategy used to build a design-oriented model are described in Section 3.

3. Towards a design-oriented lateral LFT model

In this paper, the emphasis is placed on the *lateral behavior* of the on-ground aircraft. Nevertheless, a few guidelines are provided in the concluding section to explain how the proposed modeling and control strategy can be easily extended to the longitudinal behavior.

3.1. Simplifying assumptions

Several assumptions are made to simplify the nonlinear model introduced in Section 2:

- (A_1) Inertial cross-coupling terms are neglected, which means that the inertia matrix is diagonal: $I = \text{diag}(I_{xx}, I_{yy}, I_{zz})$.
- (A_2) The runway is perfectly horizontal: there is no variation in the vertical position of the center of gravity, i.e. $V_z = 0$ and $\dot{V}_z = 0$.
- (A_3) The compressibility effects of the shock absorbers located on the landing gears are neglected. As a consequence, both pitch rate and roll rate remain constant ($p = q = 0$).
- (A_4) Due to reasonably small variations in altitude and velocity, the aerodynamic coefficients are linearized.
- (A_5) The main landing gear is reduced to a single tyre located under the fuselage, so that the aircraft only has two contact points with the runway (bicycle model). This is a fairly standard assumption in the field of active vehicle control [21,11, 18,1].
- (A_6) This paper focuses on taxiway maneuvers, which are mainly performed below 40 kts (see Section 4). The rudder thus proves almost inefficient and is not used to control the lateral motion of the aircraft.

Note that these assumptions considerably simplify the equations while preserving the quality of the model for a large class of maneuvers. The main cases for which some of them are inadequate are severe braking and differential thrust, which are not studied in this paper.

3.2. Resulting lateral equations

3.2.1. Equations of motion

According to assumptions (A_1) to (A_3), the equations of motion (1) can be simplified as follows:

$$\begin{cases} \dot{r} = \dfrac{M_z}{I_{zz}} \\ \dot{V}_y = \dfrac{F_y}{m} - rV_x \end{cases} \tag{2}$$

where r is the yaw rate and V_y the lateral velocity of the aircraft.

3.2.2. Forces and moments

Engine thrust is a purely longitudinal force. The same can be concluded for gravity according to assumptions (A_2)–(A_3). The force F_y and the moment M_z are thus only due to the aerodynamic effects and to the interactions with the ground:

$$\begin{aligned} F_y &= F_{y_a} + F_{y_g} \\ M_z &= M_{z_a} + M_{z_g} \end{aligned} \tag{3}$$

Aerodynamic effects are modeled by:

$$\begin{aligned} F_{y_a} &= \frac{1}{2}\rho S V_a^2 C_y \\ M_{z_a} &= \frac{1}{2}\rho S c V_a^2 C_n \end{aligned} \tag{4}$$

where ρ is the air density, S the reference surface of the aircraft, V_a the aerodynamic velocity and c the mean aerodynamic chord. According to assumption (A_4), the aerodynamic coefficients C_y and C_n are then linearized as follows:

$$\begin{aligned} C_y &= C_{y_\beta}\beta_a + C_{y_\delta}\delta_r + C_{y_r}\frac{rc}{V_a} \\ C_n &= C_{n_\beta}\beta_a + C_{n_\delta}\delta_r + C_{n_r}\frac{rc}{V_a} \end{aligned} \tag{5}$$

The constant terms $C_{y_\times}$ and $C_{n_\times}$ are computed from the neural networks of the initial nonlinear model and the aerodynamic sideslip angle β_a is approximated by:

$$\beta_a = \frac{V_y}{V_a} + \frac{W_y}{V_a} \tag{6}$$

where W_y denotes the lateral wind. Nevertheless, wind models are not accurate for maneuvers performed below 70 kts, so the wind input W_y is ignored here. It is then assumed that $V_a = V_x$.

Let us now focus on the lateral ground forces. They can be split up into nose wheel (NW) and main landing gear (MG) contributions:

$$F_{y_g} = F_{y_{NW}} + F_{y_{MG}} \tag{7}$$

whose expressions are further detailed in Section 3.3. They mainly depend on the local sideslip angles β_{NW} and β_{MG}, which correspond to the angles between the main velocity vector and the planes of the wheels. These angles can be modeled as follows thanks to assumption (A_5):

$$\begin{cases} \beta_{NW} = \dfrac{V_y + d_{NW} r}{V_x} - \theta_{NW} \\ \beta_{MG} = \dfrac{V_y - d_{MG} r}{V_x} \end{cases} \tag{8}$$

where d_{NW} and d_{MG} are the distances along the longitudinal axis of the aircraft between the center of gravity and the nose wheel or the main landing gear respectively.

Noting that the moment due to ground forces can be expressed as $M_{z_g} = d_{NW} F_{y_{NW}} - d_{MG} F_{y_{MG}}$, a compact parameter-varying model is finally obtained:

$$\begin{cases} \begin{bmatrix} \dot{r} \\ \dot{V}_y \end{bmatrix} = A(V_x) \begin{bmatrix} r \\ V_y \end{bmatrix} + B \begin{bmatrix} F_{y_{NW}} \\ F_{y_{MG}} \end{bmatrix} \\ \begin{bmatrix} \beta_{NW} \\ \beta_{MG} \end{bmatrix} = C(V_x) \begin{bmatrix} r \\ V_y \end{bmatrix} - \begin{bmatrix} 1 \\ 0 \end{bmatrix} \theta_{NW} \end{cases} \tag{9}$$

where the matrices $A(V_x), B$ and $C(V_x)$ can be determined by combining Eqs. (2)–(8).

3.2.3. Actuators

The engines and the wheel brakes are not modeled here, since they are only dedicated to longitudinal maneuvers. It can thus be assumed thanks to assumption (A_6) that the lateral motion of the on-ground aircraft is only controlled via the nose wheel steering system. Moreover, numerous simulations reveal that this system can be represented with a very good precision by a first-order linear model with a rate saturation:

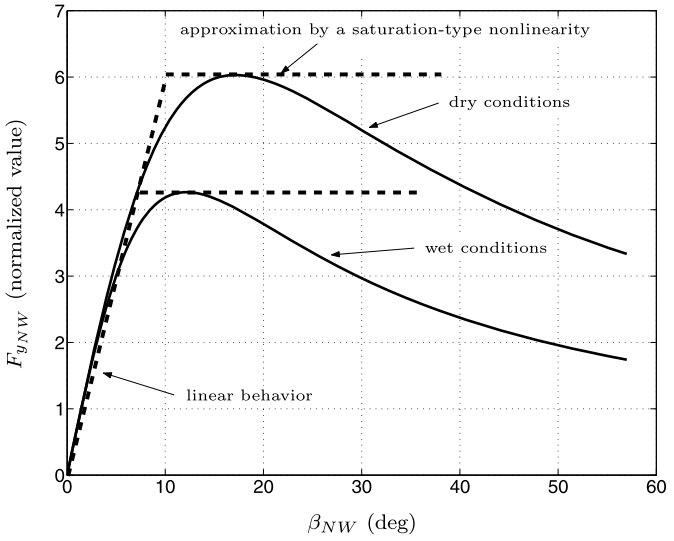

Fig. 2. Nose wheel lateral force vs β_{NW} and runway state.

$$\dot{\theta}_{NW}(t) = sat_{L_r}\big(\lambda\big(\theta_{NW_c}(t) - \theta_{NW}(t)\big)\big) \tag{10}$$

where θ_{NW_c} is the commanded nose wheel deflection, λ^{-1} the time constant, and $sat_{L_r}(.)$ a standard saturation with a unitary slope and an amplitude L_r.

3.3. Approximation of the ground forces

The key point in the modeling process is now to find a suitable expression of the lateral ground forces $F_{y_{NW}}$ and $F_{y_{MG}}$. Their dependence on the sideslip angles and the runway state is illustrated in Fig. 2 (for shortness, only the nose wheel force is shown here). It appears that these forces are close to linear functions for small sideslip angles and then reach a maximum value for an angle β_{opt} which highly depends on the runway state.

In normal operations, the control system is supposed to prevent sideslip angles from getting higher than β_{opt}. As a result, it is useless to model the ground forces for $\beta > \beta_{opt}$, at least for design purposes. This explains why, as shown in Fig. 2, these forces can be well approximated by saturation-type nonlinearities. Let us now introduce a parameter λ_{rwy} as an indicator of the runway state, as well as two positive scalars γ_{NW} and γ_{MG} referred to as the cornering gains, which correspond to the slopes of $F_{y_{NW}}$ and $F_{y_{MG}}$ in their linear regions. Forces can then be written as:

$$\begin{cases} F_{y_{NW}} \approx sat_{L_{NW}(\lambda_{rwy})}(\gamma_{NW}\beta_{NW}) \\ F_{y_{MG}} \approx sat_{L_{MG}(\lambda_{rwy})}(\gamma_{MG}\beta_{MG}) \end{cases} \tag{11}$$

3.4. Simplified LFT model of the lateral dynamics

The aerodynamic model (9), the ground forces approximation (11) and the nose wheel actuator model (10) are finally rewritten as LFR using dedicated modeling and manipulation tools [17,6,5], so as to obtain the interconnection of Fig. 3 (see [7] for further details).

The resulting simplified LFR has three states (r, V_y and the actuator state), a single input (θ_{NWc}) and two outputs (r and V_y). The associated diagonal Δ block is structured as follows:

$$\Delta = \text{diag}(\Delta_{NL}, \Delta_{LTV}) \tag{12}$$

where:

$$\begin{cases} \Delta_{NL} = \text{diag}(sat_{L_r}, sat_{L_{NW}}, sat_{L_{MG}}) \\ \Delta_{LTV} = V_x(t).I_4 \end{cases} \tag{13}$$

and I_4 is the 4-by-4 identity matrix. Note that its size has been drastically reduced compared to the initial model (see Section 2.2).

3.5. Time-domain simulations and validation

A standard on-ground maneuver is considered to evaluate the lateral model built in Section 3.4: the longitudinal velocity V_x is maintained below 20 kts and a step command is sent to the nose wheel actuator ($\theta_{NW_c} = 40°$ on a dry runway and $\theta_{NW_c} = 20°$ on a wet runway). Simulation results are shown in Fig. 4.

The simplified LFR behaves very similarly to the full nonlinear model. Moreover, its complexity remains very moderate, which makes it tractable for on-ground control laws development.

4. Design strategy

This paper focuses on lateral control laws design for the on-ground aircraft described in Section 2. More generally, the challenge is to compute a controller, which ensures a good tracking of the yaw rate r and the heading Ψ:

- with as fast a response as possible,
- without overshoot (especially in heading),
- whatever the runway state (dry, wet or icy),
- for any aircraft longitudinal on-ground velocity.

The generic procedure depicted in Fig. 5 serves as a basis for the validation of the proposed control strategy. A special attention is notably paid to the two following maneuvers:

- maneuver 1: turn to take a 30° exit while decelerating from 30 kts to 20 kts,
- maneuver 2: make a 60° turn at 10 kts.

The issue addressed in this paper is essentially a ground vehicle control problem. It has not been widely investigated in an aeronautical context [10], but considerable work has been achieved in the area of steering control for passenger cars. Many contributions deal with robust control [18,21,14], and notably H_∞ control. Gain-scheduled controllers are proposed in [4,21,14], while LFT modeling is used in [18] to structure the uncertainties and then design a robust feedforward compensator. A decoupling strategy is also proposed in [1] to reduce the influence of yaw disturbances on yaw rate and sideslip angle. A common point to these approaches is that analysis and design are mostly performed in a linear framework. The lateral ground forces are thus linearized and reduced to $F_y = \gamma\beta$, which is a reasonable assumption as long as small variations and perturbations are considered.

The objective of the present paper is quite different: the idea is to design an autopilot to improve safety, but also to minimize the maneuver time on ground. The huge variation in the ground forces with respect to the runway state (see Fig. 2) lead us to think that standard robust control methods would yield conservative results and reduced performance. The proposed approach is to perform an on-line estimation of the ground forces instead, and thus of the runway state. This information can then be used to maintain the sideslip angle just below β_{opt} during turns, so that the aircraft moves quickly without for all that slipping on the runway. In this perspective, it appears necessary to capture the nonlinear behavior of the ground forces. The direct use of the nonlinear model introduced in [2,3] is notably considered in [11], but the resulting model predictive control approach is computationally demanding and cannot be reasonably implemented in flight computers. The modeling of the lateral ground forces proposed in Section 3.3 thus appears to be a good compromise in terms of

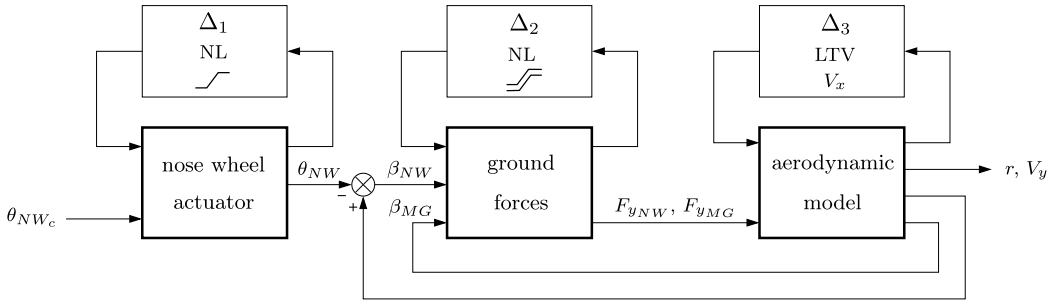

Fig. 3. Interconnexion of the different LFT models.

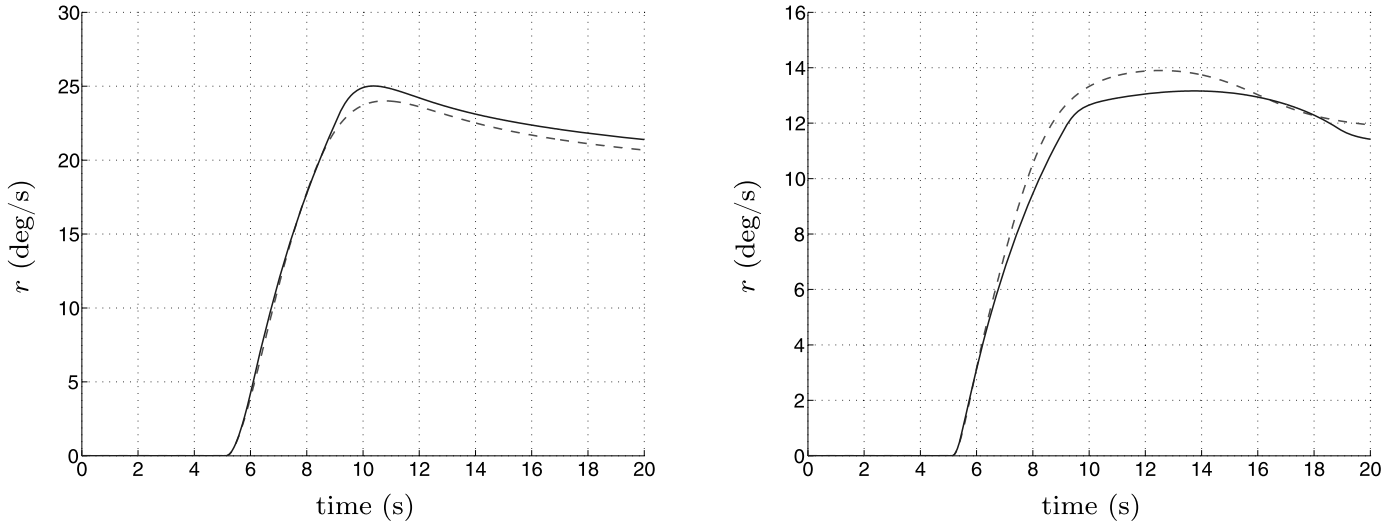

Fig. 4. On-ground aircraft behavior on dry (left) and wet (right) runways (solid lines ↔ initial nonlinear model, dashed lines ↔ simplified LFR).

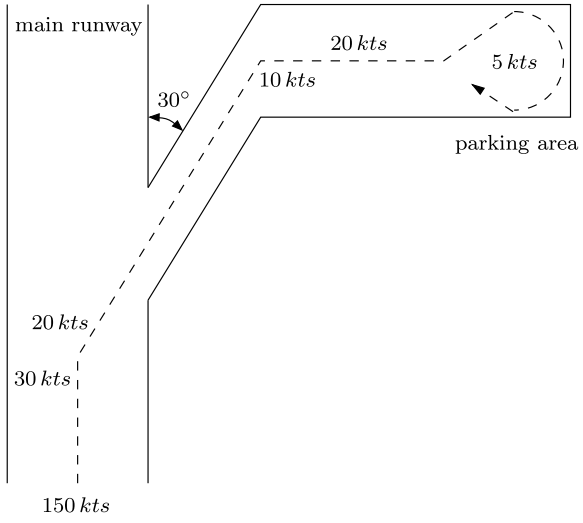

Fig. 5. Generic procedure.

both accuracy and complexity. The resulting saturations that appear in the simplified LFR depicted in Fig. 3 then strongly suggest the use of anti-windup techniques, which are further investigated in this paper. Note also that such an approach does not require to modify the nominal control laws, which is a strong industrial requirement. Indeed, an anti-windup compensator is simply added, which only acts when the sideslip angle becomes too high (see Section 6.1).

5. Anti-windup design

There exist essentially two ways in order to avoid saturation problems in systems with actuator limits. The first one, which we refer to as the one-step approach, is based – as its name implies – on a direct search for a possibly nonlinear controller which is designed from scratch. Such a controller attempts to ensure that all nominal performance specifications are met while also handling the saturation constraints imposed by the actuators. While this approach is satisfactory in principle, it leads to a difficult non-convex optimization problem. An alternative approach to the above is to perform some separation in the controller, so that one part is devoted to achieving nominal performance and the other is devoted to constraint handling. This is the approach taken in anti-windup compensation: once the nominal part of the controller has been designed, an anti-windup compensator is calculated to handle the saturation constraints. We shall not overview here all the extensive literature on this subject (see, for example, [25] for a survey of the area).

Many LMI-based approaches now exist to adjust the anti-windup gains in a systematic way. Most often, these are based on the optimization of either a stability domain [13,9], or a nonlinear $\mathcal{L}_2$-induced performance level [26,16,15]. More recently, based on the LFT/LPV framework, extended anti-windup schemes were proposed (see [23,27,16]). In these contributions, the saturations are viewed as sector nonlinearities and anti-windup controller design is recast into a convex optimization problem under LMI constraints. Following a similar path, alternative techniques using less conservative representations of the saturation nonlinearities, yet with sector nonlinearities, are proposed in [15,13,24,8].

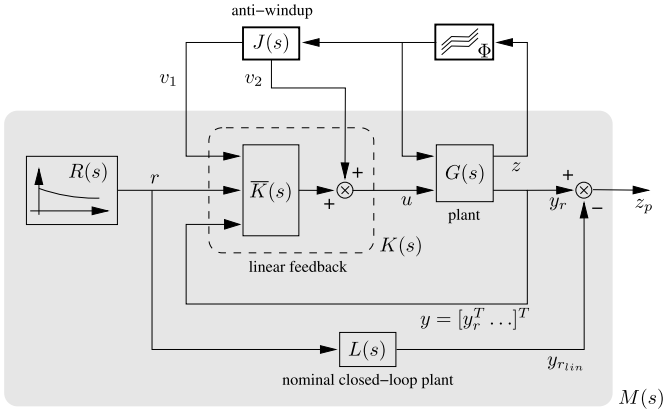

Fig. 6. Standard interconnection with a general anti-windup architecture.

The study in the sequel regards the anti-windup loop design in the LFT/LPV framework. The proposed approach extends in a less conservative way the results developed in [27] and will be applied in Section 6.

5.1. Full-order anti-windup design

Consider the nonlinear interconnection of Fig. 6. The saturated plant $G(s)$ to be controlled is written in a standard LFT form:

$$G(s):\quad \begin{cases} \dot{x}_G = A_G x_G + B_G \begin{bmatrix} \Phi(z) \\ u \end{bmatrix} \\ \begin{bmatrix} z \\ y \end{bmatrix} = C_G x_G + D_G \begin{bmatrix} \Phi(z) \\ u \end{bmatrix} \end{cases} \tag{14}$$

where u and y denote the control inputs and the measured outputs respectively.

The nonlinear operator $\Phi(.)$ in $\mathbb{R}^m$ is characterized as follows:

$$\Phi(z) = \begin{bmatrix} \phi(z_1) & \dots & \phi(z_m) \end{bmatrix}^T \tag{15}$$

where $\phi(z_i) = z_i - sat(z_i)$ is a normalized deadzone nonlinearity.

Suppose that a nominal linear controller $\overline{K}(s)$ has been first designed, so as to stabilize the plant $G(s)$ and ensure good performance properties in the linear region. To mitigate the adverse effects of saturations, additional signals v_1 and v_2 are injected both at the input and output of this controller. A state–space representation of the resulting controller $K(s)$ is then given by:

$$K(s):\quad \begin{cases} \dot{x}_K = A_K x_K + B_K y + v_1 \\ u = C_K x_K + D_K y + v_2 \end{cases} \tag{16}$$

The signals v_1 and v_2 are obtained as the outputs $v = \begin{bmatrix} v_1 \\ v_2 \end{bmatrix} \in \mathbb{R}^{n_v}$ of the dynamic anti-windup controller $J(s)$ to be determined:

$$J(s):\quad \begin{cases} \dot{x}_J = A_J x_J + B_J \Phi(z) \\ v = C_J x_J + D_J \Phi(z) \end{cases} \tag{17}$$

where the input signal $\Phi(z)$ can be interpreted as an indicator of the saturations activity.

This nonlinear closed-loop plant can be affected by some exogenous input signals r such as perturbations (wind, turbulences) or commanded inputs. In terms of performance analysis, a classical problem is to ensure that some outputs y_r of the saturated plant remain as close as possible to the outputs $y_{r_{lin}}$ of the corresponding nominal unsaturated behavior $L(s)$, which amounts to minimizing the energy of the error signal z_p. The performance level introduced in [8] allows to address this issue by restricting r to $\mathcal{L}_2$-bounded signals representative of step inputs, i.e. to the set $\mathcal{W}_\epsilon^p(\rho)$ of signals $r \in \mathbf{R}^p$ satisfying:

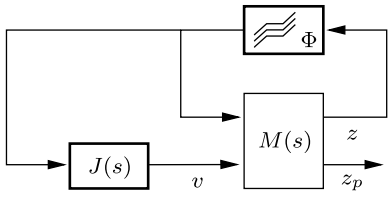

Fig. 7. A synthetic view of Fig. 6.

$$\forall t \geqslant 0, \quad r(t) = r_0 e^{-\epsilon t} \tag{18}$$

where ϵ is chosen small enough compared to the system dynamics. A stable autonomous system $R(s)$ with non-zero initial states r_0 in thus inserted into the interconnection of Fig. 6 to generate $r(t)$. Let us now define the augmented state vector ξ obtained by merging the states of the reference model (r), the nominal (linear) closed-loop system (x_L), the open-loop plant (x_G) and the nominal controller (x_K):

$$\xi = \begin{bmatrix} r \\ x_L \\ x_G \\ x_K \end{bmatrix} \in \mathbb{R}^{n_M} \tag{19}$$

The resulting system $M(s)$ connected with the anti-windup compensator is illustrated in Fig. 7 and can be defined as follows:

$$M(s):\quad \begin{cases} \dot{\xi} = A\xi + B_\phi \Phi(z) + B_a v \\ z = C_\phi \xi \\ z_p = C_p \xi + D_{p\phi} \Phi(z) + D_{pa} v = y_r - y_{r_{lin}} \in \mathbb{R}^p \end{cases} \tag{20}$$

where y_r corresponds to the first elements of the output vector $y = [y_r^T \dots]^T$.

Finally, by adding the state $x_J \in \mathbb{R}^{n_J}$ of the anti-windup compensator, the following augmented state vector is defined:

$$\nu = \begin{bmatrix} \xi \\ x_J \end{bmatrix} \in \mathbb{R}^n \tag{21}$$

and therefore the global nonlinear closed-loop plant $P(s)$ reads:

$$P(s):\quad \begin{cases} \dot{\nu} = \begin{bmatrix} A & B_a C_J \\ 0 & A_J \end{bmatrix} \nu + \begin{bmatrix} B_\phi + B_a D_J \\ B_J \end{bmatrix} \Phi(z) \\ z = [\, C_\phi \quad 0 \,] \\ z_p = [\, C_p \quad D_{pa} C_J \,]\, \nu + [\, D_{p\phi} + D_{pa} D_J \,]\, \Phi(z) \end{cases} \tag{22}$$

Let the state vector ν be partitioned as $\nu = [r^T \ \zeta^T]^T$ to distinguish more clearly the reference r from the other states $\zeta = [x_L^T \ x_G^T \ x_K^T \ x_J^T]^T \in \mathbb{R}^{n-p}$. The anti-windup design problem to be solved can then be summarized as follows:

Problem 5.1 *(Anti-windup design).* Compute a dynamic anti-windup controller $J(s)$ (i.e. matrices A_J, B_J, C_J, D_J) and a domain $\mathcal{E}(\rho)$ as large as possible such that, for a given positive scalar ρ and any reference signal $r \in \mathcal{W}_\epsilon^p(\rho)$, the following properties hold:

- the nonlinear closed-loop plant (22) is stable for all initial condition ζ_0 inside $\mathcal{E}(\rho)$,
- some outputs y_r of the plant remain as close as possible to the linear reference $y_{r_{lin}}$ (associated with the nominal unsaturated behavior), i.e. the energy of the error signal z_p is minimized.

In view of the above problem statement, the following result adapted from [8] can now be stated:

Proposition 5.2 *(Performance characterization). Consider the nonlinear interconnection of Fig. 7 with a given anti-windup controller $J(s)$. Let $u(\overline{\rho}) = [\overline{\rho} I_p \ 0]^T \in \mathbb{R}^{n \times p}$. If there exist matrices $Q = Q^T \in \mathbb{R}^{n \times n}$,*

$S = \mathrm{diag}(s_1, \ldots, s_m)$, $Z \in \mathbb{R}^{m\times n}$ *and positive scalars* γ *and* $\overline{\rho}$ *such that the following LMI conditions hold (where* Z_i *and* $C_{\phi i}$ *denote the* i^{th} *rows of* Z *and* C_ϕ *respectively)*[2]:

$$\begin{pmatrix} Q & \star \\ u(\overline{\rho})^T & I_p \end{pmatrix} > 0 \tag{23}$$

$$\begin{pmatrix} \begin{bmatrix} A & B_a C_J \\ 0 & A_J \end{bmatrix} Q + Q \begin{bmatrix} A & B_a C_J \\ 0 & A_J \end{bmatrix}^T & \star & \star \\ S \begin{bmatrix} B_\phi + B_a D_J \\ B_J \end{bmatrix}^T - Z & -2S & \star \\ [\, C_p \quad D_{pa} C_J \,] Q & [\, D_{p\phi} + D_{pa} D_J \,] S & -\gamma I_p \end{pmatrix} < 0 \tag{24}$$

$$\begin{pmatrix} Q & \star \\ Z_i + [\, C_{\phi_i} \quad 0 \,] Q & 1 \end{pmatrix} > 0, \quad i = 1, \ldots, m \tag{25}$$

then for all $\rho \leqslant \overline{\rho}$ *and all reference signals* $r \in \mathcal{W}_\epsilon^p(\rho)$, *the nonlinear interconnected system (22) is stable for all initial condition* ζ_0 *in the domain* $\mathcal{E}(\rho)$ *defined as follows*:

$$\mathcal{E}(\rho) = \left\{ \zeta \in \mathbb{R}^{n-p}; \forall r \in \mathcal{W}_\epsilon^p(\rho), \begin{bmatrix} r \\ \zeta \end{bmatrix}^T P \begin{bmatrix} r \\ \zeta \end{bmatrix} \leqslant 1 \right\} \tag{26}$$

where $P = Q^{-1}$. *Moreover, the output energy satisfies*:

$$\int_0^\infty z_p(t)^T z_p(t)\, dt \leqslant \gamma \tag{27}$$

Let us now focus on the anti-windup design issue stated in Problem 5.1. In this case, the decision variable Q introduced in Proposition 5.2 and the state–space matrices of $J(s)$ have to be computed simultaneously. As a result, inequality (24) becomes a BMI and is thus no longer convex. However, in the full-order case (i.e. $n_J = n_M$), the constraints (23)–(25) exhibit particular structures which can be exploited to derive a convex characterization.

Proposition 5.3 *(Full-order anti-windup design). Consider the nonlinear interconnection of Fig. 7. Let* $\Gamma = \mathrm{diag}(N_a, I_m, N_{pa})$, *where* N_a *and* N_{pa} *denote any basis of the null-spaces of* B_a^T *and* D_{pa}^T *respectively. Let* $v(\overline{\rho}) = [\overline{\rho} I_p 0]^T \in \mathbb{R}^{n_M \times p}$. *There exists an anti-windup controller* $J(s)$ *such that the conditions of Proposition 5.2 are satisfied if and only if there exist matrices* $X = X^T, Y = Y^T \in \mathbb{R}^{n_M \times n_M}$, $S = \mathrm{diag}(s_1, \ldots, s_m)$ *and* $W = [U \; V] \in \mathbb{R}^{m\times(n_M+n_M)}$ *such that the following LMI conditions hold*:

$$v(\overline{\rho})^T X v(\overline{\rho}) < I_p \tag{28}$$

$$\begin{pmatrix} A^T X + X A & \star \\ C_p & -\gamma I_p \end{pmatrix} < 0 \tag{29}$$

$$\Gamma^T \begin{pmatrix} AY + Y A^T & \star & \star \\ S B_\phi^T - V & -2S & \star \\ C_p Y & 0 & -\gamma I_p \end{pmatrix} \Gamma < 0 \tag{30}$$

$$\begin{pmatrix} X & \star & \star \\ I_{n_M} & Y & \star \\ U_i & V_i + C_{\phi_i} Y & 1 \end{pmatrix} > 0, \quad i = 1, \ldots, m \tag{31}$$

Sketch of proof. Following a scheme proposed by [12], it suffices to rewrite inequalities (23)–(25) of Proposition 5.2 by capturing the decision variables A_J, B_J, C_J and D_J into a single matrix Ω, which can then be eliminated using the projection lemma. □

[2] For compactness, the symmetric terms in the matrix inequalities are replaced by "$\star$" throughout.

Remark 5.4. The matrix Q of Proposition 5.2 is obtained from X and Y as follows [12]:

$$Q = \begin{pmatrix} Y & I_{n_M} \\ N & 0 \end{pmatrix} \begin{pmatrix} I_{n_M} & X \\ 0 & M \end{pmatrix}^{-1} \quad \text{where } M^T N = I_{n_M} - XY \tag{32}$$

The decision variable Q being fixed, inequality (24) is convex with respect to the state–space matrices A_J, B_J, C_J and D_J of the anti-windup controller, which can thus be easily computed.

5.2. Fixed-order anti-windup design

Fixing the matrix A_J is a convenient way to control precisely the dynamics of the anti-windup controller. Moreover, as stated in Proposition 5.5 below, when C_J is also fixed, the anti-windup problem becomes convex even if $n_J < n_M$.

Proposition 5.5. *The BMI constraint (24) of Proposition 5.2 is convex as soon as the matrices* A_J *and* C_J *of the anti-windup controller are fixed.*

Proof. It immediately follows from a classical change of variables $\tilde{B}_J = B_J S$ and $\tilde{D}_J = D_J S$, which is here valid since $S > 0$. □

Based on this result, the following algorithm is introduced:

Algorithm 1 *(Fixed-dynamics anti-windup design).*

1. Choose appropriate A_J and C_J matrices, which define respectively the state and the output matrices of the anti-windup controller $J(s)$ to be computed.
2. Fix $\overline{\rho}$ and minimize γ under the LMI constraints (23)–(25) w.r.t. Q, S, Z, $\tilde{B}_J$ and $\tilde{D}_J$.
3. Compute B_J and D_J by inverting the aforementioned change of variables.

The main difficulty in the above algorithm consists in choosing the matrices A_J and C_J correctly. This choice may appear more intuitive and natural by considering the following decomposition:

$$J(s) = M_0 + \sum_{i=1}^{n_1} \frac{M_{i1}}{s + \lambda_i} + \sum_{i=1}^{n_2} \frac{M_{i2}}{s^2 + 2\eta_i\omega_i s + \omega_i^2} \tag{33}$$

where $D_J = M_0$ and B_J contains the collections of matrices M_{i1} and M_{i2}. For this decomposition, the fixed matrices A_J and C_J can be chosen as:

$$\begin{aligned} A_J &= \mathrm{diag}(-\lambda_1, \ldots, -\lambda_{n_1}, A_1, \ldots, A_{n_2}) \\ C_{J_k} &= [\underbrace{1 \ldots 1}_{n_1} \underbrace{[1\,0] \ldots [1\,0]}_{n_2}], \quad k = 1, \ldots, n_v \end{aligned} \tag{34}$$

where:

$$A_i = \begin{pmatrix} 0 & 1 \\ -\omega_i^2 & -2\eta_i\omega_i \end{pmatrix}, \quad i = 1, \ldots, n_2 \tag{35}$$

From this observation, the first step of Algorithm 1 simply boils down to the choice of a list of poles for the anti-windup controller, whose matrices A_J and C_J are then immediately deduced from (34) and (35).

Remark 5.6. The poles of the reduced-order anti-windup controller can be chosen by selecting some of those obtained in the full-order case. Typically, very slow and fast dynamics are eliminated. Alternatively, an iterative procedure starting from the static case can be implemented: the list of poles is progressively enriched until the gap between the full and reduced-order cases becomes small enough.

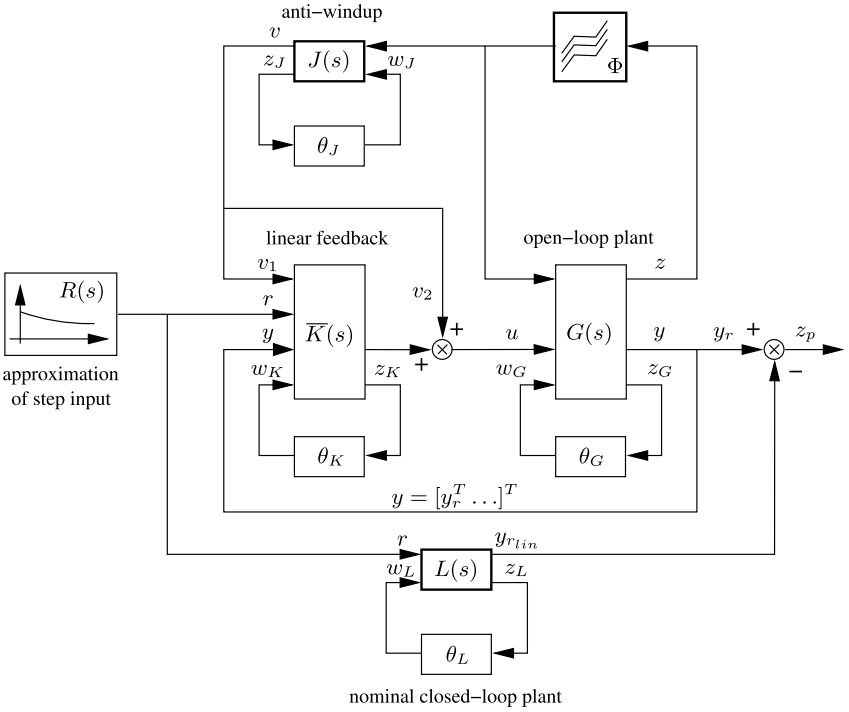

Fig. 8. Description of the general parameter-dependent anti-windup architecture.

5.3. Extension to parameter-varying systems

5.3.1. Description of the problem

The nonlinear interconnection considered in this section and depicted in Fig. 8 is similar to the one described in Section 5.1, except that the saturated plant $G(s)$ now depends on real time-varying parameters $\delta_1(t),\dots,\delta_k(t)$. More precisely, for each $t \geqslant 0$, $\theta_G(t)$ is a block-diagonal operator specifying how these parameters enter the plant dynamics, i.e. $w_G = \theta_G(t) z_G$, where:

$$\theta_G(t) = \operatorname{diag}\big(\delta_1(t) I_{l_1},\dots,\delta_k(t) I_{l_k}\big) \tag{36}$$

The operator $\theta_G(t)$ is normalized, i.e. $\theta_G(t)^T\theta_G(t) \leqslant I_l$, where $l = l_1 + \cdots + l_k$. The set of all normalized operators with structure (36) is denoted by Θ_G, and thus $\theta_G(t) \in \Theta_G\ \forall t \geqslant 0$.

Similarly, the nominal controller $\overline{K}(s)$, the nominal closed-loop plant $L(s)$ and the anti-windup controller $J(s)$ all depend on real time-varying parameters. The associated normalized block-diagonal operators are denoted by $\theta_K(t), \theta_L(t)$ and $\theta_J(t)$ respectively. In this context, the augmented plant $M(s)$ introduced in Section 5.1 can now be described by:

$$M(s):\quad \begin{cases} \dot\xi = A\xi + B_\phi \Phi(z) + B_a v + B_\theta w_M \\ z = C_\phi \xi \\ z_p = C_p\xi + D_{p\phi}\Phi(z) + D_{pa} v + D_{p\theta} w_M \\ z_M = C_\theta \xi + D_{\theta\phi}\Phi(z) + D_{\theta a} v + D_{\theta\theta} w_M \\ w_M = \theta_M(t) z_M \end{cases} \tag{37}$$

where

$$\theta_M(t) = \operatorname{diag}\big(\theta_L(t), \theta_G(t), \theta_K(t)\big) \in \Theta_M \subset \mathbb{R}^{p_M \times p_M} \tag{38}$$

The parameter-dependent anti-windup controller $J(s)$ to be computed is then given by:

$$J(s):\quad \begin{cases} \dot x_J = A_J x_J + B_{J\phi}\Phi(z) + B_{J\theta} w_J \\ v = C_{Ja} x_J + D_{Ja\phi}\Phi(z) + D_{Ja\theta} w_J \\ z_J = C_{J\theta} x_J + D_{J\theta\phi}\Phi(z) + D_{J\theta\theta} w_J \end{cases} \tag{39}$$

The global nonlinear closed-loop plant $P(s)$ including $J(s)$ is finally obtained as follows:

$$P(s):\quad \begin{cases} \dot\nu = \mathcal{A}\nu + \mathcal{B}_\phi \Phi(z) + \mathcal{B}_\theta w_\theta \\ z = \mathcal{C}_\phi \nu \\ z_p = \mathcal{C}_p \nu + \mathcal{D}_{p\phi}\Phi(z) + \mathcal{D}_{p\theta} w_\theta \\ z_\theta = \mathcal{C}_\theta \nu + \mathcal{D}_{\theta\phi}\Phi(z) + \mathcal{D}_{\theta\theta} w_\theta \\ w_\theta = \theta(t) z_\theta \end{cases} \tag{40}$$

where

$$\theta(t) = \operatorname{diag}\big(\theta_M(t), \theta_J(t)\big) \in \Theta_P \subset \mathbb{R}^{p_P \times p_P} \tag{41}$$

and

$$\begin{pmatrix} \mathcal{A} & \mathcal{B}_\phi & \mathcal{B}_\theta \\ \mathcal{C}_\phi & 0 & 0 \\ \mathcal{C}_p & \mathcal{D}_{p\phi} & \mathcal{D}_{p\theta} \\ \mathcal{C}_\theta & \mathcal{D}_{\theta\phi} & \mathcal{D}_{\theta\theta} \end{pmatrix} = \left(\begin{array}{cc|c|cc} A & B_a C_{Ja} & B_\phi + B_a D_{Ja\phi} & B_\theta & B_a D_{Ja\theta} \\ 0 & A_J & B_{J\phi} & 0 & B_{J\theta} \\ \hline C_\phi & 0 & 0 & 0 & 0 \\ \hline C_p & D_{pa} C_{Ja} & D_{p\phi} + D_{pa} D_{Ja\phi} & D_{p\theta} & D_{pa} D_{Ja\theta} \\ \hline C_\theta & D_{\theta a} C_{Ja} & D_{\theta\phi} + D_{\theta a} D_{Ja\phi} & D_{\theta\theta} & D_{\theta a} D_{Ja\theta} \\ 0 & C_{J\theta} & D_{J\theta\phi} & 0 & D_{J\theta\theta} \end{array}\right)$$

5.3.2. Parameter-varying anti-windup design

Let $\mathcal{S}_x$ be the convex set of positive definite scaling matrices that commute with every operator θ of a given set Θ_x:

$$\mathcal{S}_x = \big\{ L = L^T > 0 :\ L\theta = \theta L\ \forall \theta \in \Theta_x \big\}$$

where $x \in \{P, M\}$ in the sequel. On the basis of the above context, Proposition 5.2 is adapted to deal with time-varying parameters. Inequality (24) is simply replaced by:

$$\begin{pmatrix} \mathcal{A}Q + Q\mathcal{A}^T & \star & \star & \star & \star \\ S\mathcal{B}_\phi^T - Z & -2S & \star & \star & \star \\ \mathcal{C}_p Q & \mathcal{D}_{p\phi} S & -\gamma I_p & \star & \star \\ L\mathcal{B}_\theta^T & 0 & L\mathcal{D}_{p\theta}^T & -L & \star \\ \mathcal{C}_\theta Q & \mathcal{D}_{\theta\phi} S & 0 & \mathcal{D}_{\theta\theta} L & -L \end{pmatrix} < 0 \tag{42}$$

where $L \in \mathcal{S}_P$. Let us now focus on the anti-windup design issue. In this case, the analysis variable Q and the state–space matrices of $J(s)$ have to be optimized simultaneously. As a result, inequality (42) is no longer convex, unless the following assumptions are satisfied:

- full-order anti-windup controllers are designed, i.e. $n_J = n_M$,
- the structures of $\theta_J(t)$ and $\theta_M(t)$ are the same, i.e. $\theta_J(t) = \theta_M(t) \forall t \geqslant 0$.

Proposition 5.3 can then be adapted to deal with time-varying parameters. Let $\Gamma = \mathrm{diag}(N_a, I_m, N_{pa}, I_{2p_M}, N_{\theta a})$, where N_a, N_{pa} and $N_{\theta a}$ denote any basis of the null-spaces of B_a^T, D_{pa}^T and $D_{\theta a}^T$ respectively. Inequalities (29) and (30) are replaced by:

$$\begin{pmatrix} A^TX + XA & \star & \star & \star & \star \\ C_p & -\gamma I_p & \star & \star & \star \\ B_\theta^T X & D_{p\theta}^T & -I_{n_M} & \star & \star \\ TC_\theta & 0 & TD_{\theta\theta} & -T & \star \\ C_\theta & 0 & D_{\theta\theta} & -I_{n_M} & -R \end{pmatrix} < 0 \tag{43}$$

$$\Gamma^T \begin{pmatrix} AY + YA^T & \star & \star & \star & \star & \star \\ SB_\phi^T - V & -2S & \star & \star & \star & \star \\ C_pY & D_{p\phi}S & -\gamma I_p & \star & \star & \star \\ RB_\theta^T & 0 & RD_{p\theta}^T & -R & \star & \star \\ B_\theta^T & 0 & D_{p\theta}^T & -I_{n_M} & -T & \star \\ C_\theta Y & D_{\theta\phi}S & 0 & D_{\theta\theta}R & D_{\theta\theta} & -R \end{pmatrix} \Gamma < 0 \tag{44}$$

where $R, T \in \mathcal{S}_M$. Similarly, the approach of Section 5.2 can be applied in the present context.

6. Application to the on-ground control problem

Let us now focus again on the on-ground aircraft application. Using the method described in Section 5, an anti-windup controller is first designed in Section 6.1 from the simplified LFR of Section 3, so as to satisfy the design specifications detailed in Section 4. Sections 6.2 and 6.3 are then dedicated to the practical implementation of the resulting controller on the full nonlinear model introduced in Section 2. A few simulation results are finally presented in Section 6.4 to demonstrate the efficiency of the design scheme.

6.1. Anti-windup design from the simplified LFR

A two-step design procedure is proposed. A nominal controller depending on the aircraft longitudinal velocity V_x is first designed, so as to ensure good stability and performance properties when no saturations are active. It is classically composed of both an inner loop for yaw rate control and an outer loop for heading control. The second step then consists in designing an anti-windup compensator, which also depends on V_x and acts on the nominal controller to reduce the negative effects of the saturations.

6.1.1. Inner loop

Let us first focus on the yaw rate control, also called the inner control loop. The saturations are temporarily ignored and a nominal proportional-integral (PI) controller $K_r(s)$ depending on the aircraft longitudinal velocity V_x is designed by a modal technique using the LFR Toolbox for Matlab [17]. The resulting closed-loop plant is depicted in Fig. 9, where H is a constant feedforward gain and K a third-order rational function in V_x. It behaves like a well-damped second-order system with a pulsation $\omega_r = 2.15$ rad/s for any aircraft longitudinal velocity below 40 kts. Note that this is the minimum order which guarantees that ω_r remains constant on the whole speed range.

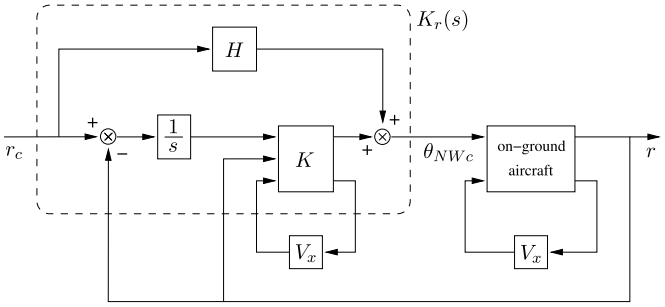

Fig. 9. Structure of the nominal parameter-varying PI controller.

The commanded yaw rate r_c is tracked without steady-state error, but an important overshoot occurs when the saturations are active, as shown by the dotted line in Fig. 13. This overshoot cannot be eliminated unless the pulsation of the PI controller is significantly reduced, resulting in an excessively slow response time. The next step thus consists of designing a parameter-varying anti-windup compensator (function of V_x) to take into account the adverse effects of the saturations. As pointed out in Section 5, this issue reduces to the minimization of a linear objective (the performance index) under LMI constraints. Several controllers are computed for various runway conditions, i.e. for various saturation levels, using the method described in Section 5. It finally appears that an anti-windup controller J_r optimized for wet runway conditions offers a good compromise.

6.1.2. Outer loop

The commanded yaw rate r_c can be directly sent to the inner loop by the pilot through the use of a dedicated control device, such as a side-stick tiller. But it can also be provided by an autopilot in charge of controlling the aircraft heading: this is the outer loop. The associated controller $K_\Psi(s)$ is a first-order system, whose gain, zero and pole are first, second and second-order rational functions of V_x respectively. This guarantees that the dominant mode is about 1.2 rad/s when no saturations are active. The closed-loop plant with both inner and outer controllers is shown in Fig. 10.

6.2. On-line estimation of the ground forces

The next step is to implement this anti-windup controller on the full nonlinear model described in Section 3. The main difficulty is that the saturation levels depend on the ground forces, whose characteristics are strongly affected by the runway state and the vertical load. It is thus necessary to identify these forces on-line. An identification procedure is proposed, which is based on the dynamic inversion of the lateral linear parameter varying (LPV) model (9). More precisely, using the notation below:

- $x_{NL} = [r_{NL}\ V_{y_{NL}}]^T$: state vector of the full nonlinear model,
- $x_{LPV} = [r_{LPV} V_{y_{LPV}}]^T$: state vector of the LPV model,

and following along the same lines as in [22], the lateral ground forces are estimated by:

$$\begin{bmatrix} \hat{F}_{y_{NW}} \\ \hat{F}_{y_{MG}} \end{bmatrix} \approx B^{-1}\big[\alpha I - A(V_x)\big] \begin{bmatrix} x_{NL} - x_{LPV} \\ x_{LPV} \end{bmatrix} \tag{45}$$

where α is a positive scalar which is chosen sufficiently large compared to the aircraft dynamics. As shown in Fig. 2, the saturations are active as soon as the estimated ground forces are less than

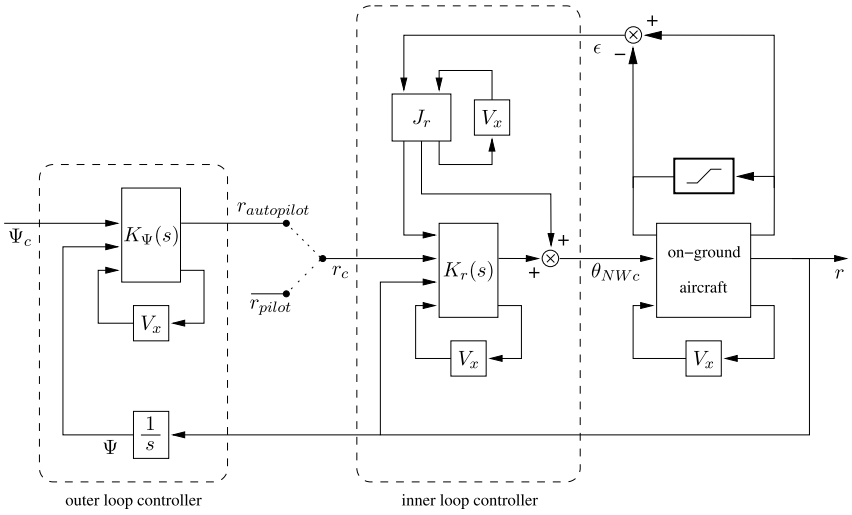

Fig. 10. Overall structure of the closed-loop plant.

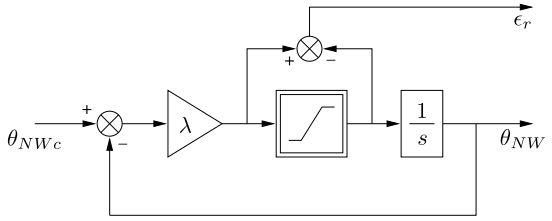

Fig. 11. Estimation of the nose wheel steering system saturation level.

their linear approximation. The saturations levels can thus be estimated using Eqs. (9) and (45) via two signals ϵ_{NW} and ϵ_{MG}:

$$\begin{cases} \epsilon_{NW} = \text{sign}(\beta_{NW})|\hat{F}_{y_{NW}} - \gamma_{NW}\beta_{NW}| \\ \epsilon_{MG} = \text{sign}(\beta_{MG})|\hat{F}_{y_{MG}} - \gamma_{MG}\beta_{MG}| \end{cases} \tag{46}$$

Let us now combine this estimator with the nose wheel steering system model described by Fig. 11. Using LFT modeling, a global estimator is finally obtained, whose outputs ϵ_r, ϵ_{NW} and ϵ_{MG} exhibit non-zero values when the corresponding saturations are active and can be directly used by an anti-windup control device.

6.3. LFT-based implementation of the controller

The resulting adaptive controller is composed of both the parameter-varying anti-windup controller computed in Section 6.1 and the aforementioned estimator block. It is implemented on the full nonlinear model as shown in Fig. 12.

It is worth pointing out that this controller is given in an LFT format and can thus be easily implemented on-line. Moreover, both its order (6) and the repetition of V_x in the Δ block (16) remain low.

6.4. Simulation results

Fig. 13 shows the response of the on-ground aircraft to a yaw rate step input on a wet runway and for a longitudinal velocity $V_x \approx 8$ m/s. The input signal is drawn as a thin solid line. Without anti-windup compensation (dotted line), the PI controller ensures that there is no steady-state error but a strong overshoot can be observed, and it takes almost 8 seconds to reach the desired value. If only the anti-windup compensator associated with the rate limitation of the nose wheel steering system is implemented (dashed line), the overshoot is significantly reduced. Finally, with full anti-windup compensation (solid line), the reference input is perfectly tracked in little more than 3 s with a negligible overshoot, which conforms to the design specifications expressed in Section 4. It appears that each term brings its own contribution, thus showing the relevance of the proposed multidimensional anti-windup scheme.

Let us now consider the two specific maneuvers detailed in Section 4. The emphasis is placed on the yaw rate control, which is more commonly used in practice by pilots. Each simulation proceeds as follows from a piloting point of view:

- a yaw rate step input with a suitable amplitude is first applied to start the turn,
- the yaw rate input is set back to zero when needed to reach the desired heading.

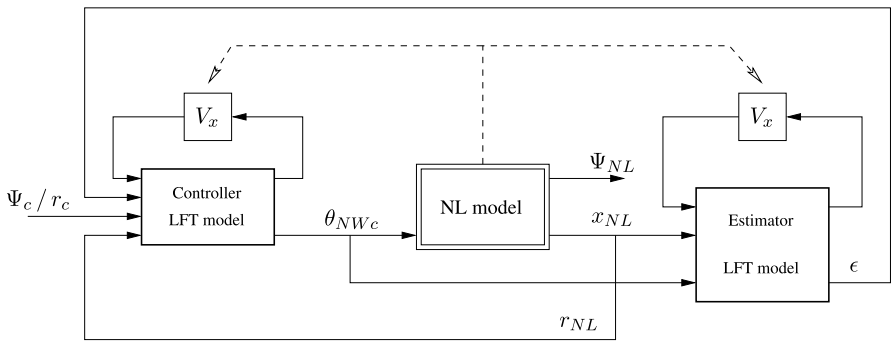

Fig. 12. Controller integration on the full nonlinear model.

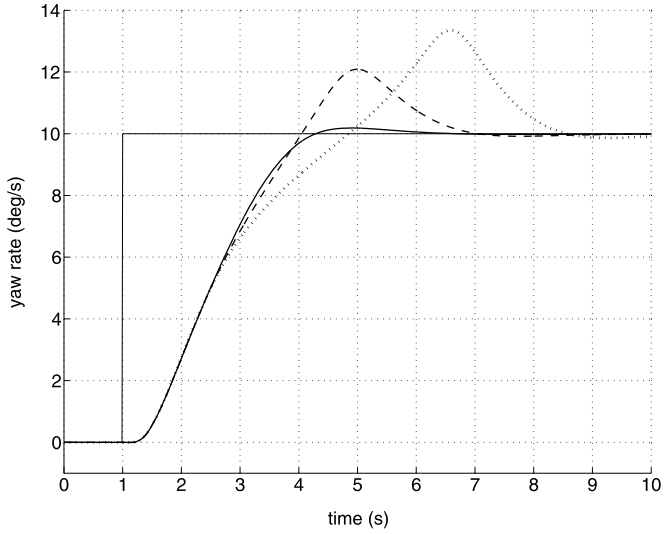

Fig. 13. Step responses with no, partial and full anti-windup compensation.

The basic idea underlying this piloting strategy is to consider only simple commanded inputs, which can be easily applied by a human pilot. Simulations are performed for various runway conditions (dry, wet, icy) are results are shown in Figs. 14 and 15.

The anti-windup signal becomes non-zero as soon as one of the saturations is active. The orders that are sent to the control effectors are thus alleviated when the sideslip angles become too high, which prevents the aircraft from slipping on the ground. Note that in most cases, the closed-loop plant is unstable without anti-windup compensation. Moreover, the shape and the response time are satisfactory whatever the runway conditions, which demonstrates the ability of the on-line estimator to identity the ground forces, i.e. the runway state. It thus appears that the heading is perfectly controlled whatever the runway state and the aircraft longitudinal velocity, which conforms to the design specifications and proves the effectiveness of the proposed parameter-dependent anti-windup controller.

7. Conclusion

This paper deals with the lateral control of an on-ground transport aircraft. A simplified design-oriented representation is first obtained from a high-fidelity nonlinear model developed in an industrial context. The key step of this modeling process consists in reducing the highly nonlinear ground forces to saturation-type nonlinearities. Despite its simplicity, it appears that the resulting model performs very well on a large operating domain. An original parameter-varying anti-windup control design technique is then developed and successfully applied in a non-conventional context. In most anti-windup applications indeed, the saturations typically appear on the actuators dynamics and are well identified. But in this work, they are used to represent the nonlinear ground forces, whose magnitudes strongly depend on the runway state. Consequently, such saturations are a priori unknown and have to be identified on-line. As shown in this contribution, this operation can be handled by an LFT-based estimator. An adaptive parameter-varying anti-windup controller is thus obtained, and can be easily implemented thanks to its LFT structure. Nonlinear simulations prove the efficiency of the proposed methodology to handle low-speed lateral maneuvers whatever the runway state (from nominal to icy conditions). Thanks to the anti-windup action, the nose wheel control system is fully exploited at all times, without any risk. This results in highly optimized yaw rate and heading responses.

It should be emphasized that the proposed approach could be extended to handle a higher velocity range, and thus to cover any possible on-ground maneuver from touchdown to complete stop. In this case, the aerodynamic forces play an important role and the on-ground aircraft has to be controlled with both the rudder and the nose wheel steering system. The crucial point is thus to find a suitable way to share the control action between these two devices according to the aircraft velocity, either by using an allocation module or by performing a multi-inputs design. Note that the LFR developed in Section 3.4 can be directly exploited, since it already takes into account the aerodynamic effects. As a final point, note that a similar methodology could be applied to control the longitudinal dynamics of the on-ground aircraft, since the longitudinal ground forces can also be modeled by saturation-type nonlinearities.

Acknowledgement

The authors would like to thank Charles Poussot-Vassal (ONERA) for his contribution to the short survey on ground vehicle control.

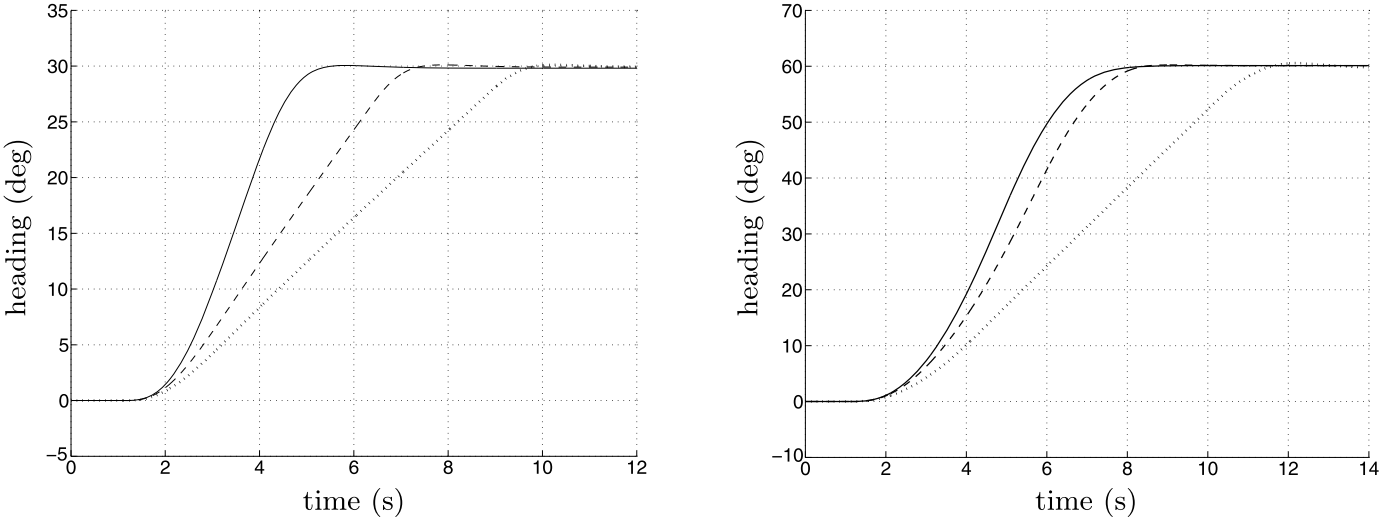

Fig. 14. Heading responses (left ↔ maneuver 1, right ↔ maneuver 2) for dry (solid line), wet (dashed line) and icy (dotted line) runways.

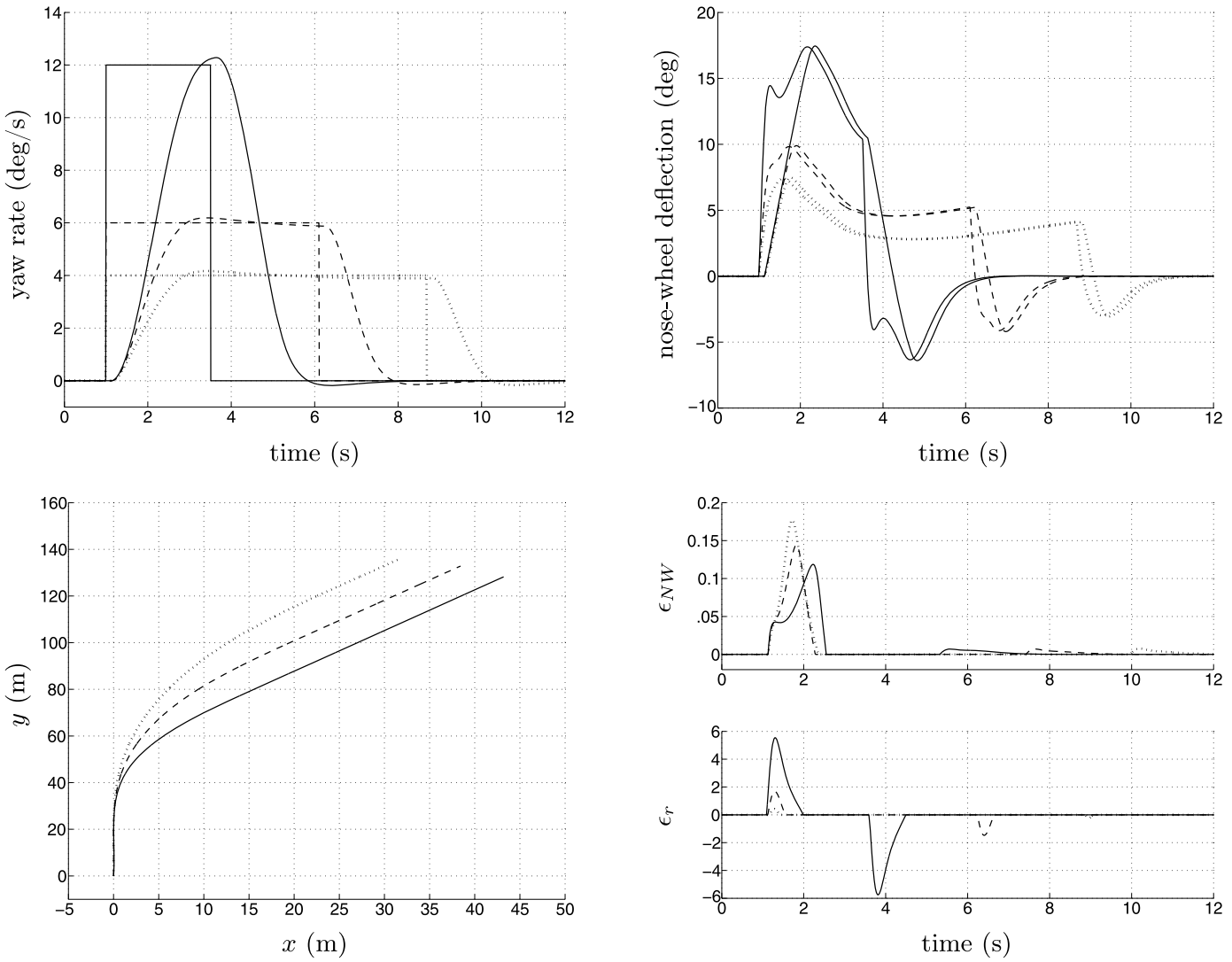

Fig. 15. Commanded and achieved yaw rates (upper left) and nose wheel deflections (upper right), aircraft trajectories (lower left) and saturations activity (lower right) for dry (solid lines), wet (dashed lines) and icy (dotted lines) runways (maneuver 1).

References

[1] J. Ackermann, T. Bünte, Yaw disturbance attenuation by robust decoupling of car steering, in: Proceedings of the 13th IFAC World Congress, San Francisco, California, 1996, pp. 1–6.

[2] E. Bakker, L. Nyborg, H. Pacejka, Tyre modelling for use in vehicle dynamic studies, in: Proceedings of the SAE International Congress and Expo, Detroit, USA, 1987, paper 870421.

[3] A. Barnes, T. Yager, Enhancement of aircraft ground handling simulation capability, Advisory Group for Aerospace Research and Development, AGARDograph 333.

[4] S. Baslamisli, I. Kose, G. Anlas, Gain-scheduled integrated active steering and differential control for vehicle handling improvement, Vehicle System Dynamics 47 (1) (2009) 99–119.

[5] J.-M. Biannic, C. Döll, Simulink handling of LFR objects, available at http://www.cert.fr/dcsd/idco/perso/Biannic/mypage.html, 2006.

[6] J.-M. Biannic, C. Döll, J.-F. Magni, Simulink-based tools for creating and simulating interconnected LFR objects, in: Proceedings of the IEEE International Symposium on Computer Aided Control Systems Design, Munich, Germany, 2006, pp. 1922–1927.

[7] J.-M. Biannic, A. Marcos, M. Jeanneau, C. Roos, Nonlinear simplified LFT modelling of an aircraft on ground, in: Proceedings of the IEEE Conference on Control Applications, Munich, Germany, 2006, pp. 2213–2218.

[8] J.-M. Biannic, S. Tarbouriech, D. Farret, A practical approach to performance analysis of saturated systems with application to fighter aircraft flight controllers, in: Proceedings of the 5th IFAC Symposium on Robust Control Design, Toulouse, France, 2006.

[9] Y. Cao, Z. Lin, D. Ward, An antiwindup approach to enlarging domain of attraction for linear systems subject to actuator saturation, IEEE Transactions on Automatic Control 47 (1) (2002) 140–145.

[10] J. Duprez, F. Mora-Camino, F. Villaume, Aircraft-on-ground lateral control for low speed manœuvers, in: Proceedings of the 16th IFAC Symposium on Automatic Control in Aerospace, St. Petersburg, Russia, 2004.

[11] P. Falcone, F. Borrelli, J. Asgari, H. Tseng, D. Hrovat, Predictive active steering control for autonomous vehicle systems, IEEE Transactions on Control Systems Technology 15 (3) (2007) 566–580.

[12] P. Gahinet, P. Apkarian, A linear matrix inequality approach to H_∞ control, International Journal of Robust and Nonlinear Control 4 (1994) 421–448.

[13] J. Gomes da Silva Jr., S. Tarbouriech, Anti-windup design with guaranteed region of stability: an LMI-based approach, IEEE Transactions on Automatic Control 50 (1) (2005) 106–111.

[14] B. Güvenc, T. Bünte, D. Odenthal, L. Güvenc, Robust two degree-of-freedom vehicle steering controller design, IEEE Transactions on Control Systems Technology 12 (4) (2004) 627–636.

[15] T. Hu, A. Teel, L. Zaccarian, Regional anti-windup compensation for linear systems with input saturation, in: Proceedings of the American Control Conference, Portland, USA, 2005, pp. 3397–3402.

[16] B. Lu, F. Wu, S. Kim, Linear parameter varying anti-windup compensation for enhanced flight control performance, AIAA Journal of Guidance, Control and Dynamics 28 (3) (2005) 494–504.

[17] J.-F. Magni, Linear Fractional Representation Toolbox (version 2.0) for use with Matlab, available at http://www.cert.fr/dcsd/idco/perso/Magni/, 2006.

[18] S. Mammar, D. Koenig, Vehicle handling improvement by active steering, Vehicle System Dynamics 38 (3) (2002) 211–242.
[19] A. Marcos, D. Bates, I. Postlethwaite, Exact nonlinear modelling using symbolic linear fractional transformations, in: Proceedings of the 16th IFAC World Congress, Prague, Czech Republic, 2005.
[20] A. Marcos, J.-M. Biannic, M. Jeanneau, D. Bates, I. Postlethwaite, Aircraft modelling for nonlinear and robust control design and analysis, in: Proceedings of the 5th IFAC Symposium on Robust Control Design, Toulouse, France, 2006.
[21] C. Poussot-Vassal, O. Sename, L. Dugard, Robust vehicle dynamic stability controller involving steering and braking systems, in: Proceedings of the 9th European Control Conference, Budapest, Hungary, 2009.
[22] C. Roos, J.-M. Biannic, Aircraft-on-ground lateral control by an adaptive LFT-based anti-windup approach, in: Proceedings of the IEEE Conference on Control Applications, Munich, Germany, 2006, pp. 2207–2212.
[23] M. Saeki, N. Wada, Synthesis of a static anti-windup compensator via linear matrix inequalities, International Journal of Robust and Nonlinear Control 12 (10) (2002) 927–953.
[24] S. Tarbouriech, I. Queinnec, G. Garcia, Stability region enlargement through anti-windup strategy for linear systems with dynamics restricted actuator, International Journal of System Science 37 (2) (2006) 79–90.
[25] S. Tarbouriech, M. Turner, Anti-windup design: an overview of some recent advances and open problems, IET Control Theory and Application 3 (1) (2009) 1–19.
[26] M. Turner, S. Tarbouriech, Anti-windup for linear systems with sensor saturation: sufficient conditions for global stability and L2 gain, in: Proceedings of the 45th IEEE Conference on Decision and Control, San Diego, USA, 2006, pp. 5418–5423.
[27] F. Wu, M. Soto, Extended anti-windup control schemes for LTI and LFT systems with actuator saturations, International Journal of Robust and Nonlinear Control 14 (15) (2004) 1255–1281.